UNIVERSITY OF BIRMINGHAM
University of Birmingham Research at Birmingham

The effect of deposition conditions on atmospheric pitting corrosion location under Evans droplets on 304L stainless steel

Street, Steven; Cook, Angus; Mohammed Ali, Haval; Rayment, Trevor; Davenport, Alison

DOI:
10.5006/2614

License:
None: All rights reserved

Document Version
Peer reviewed version

Citation for published version (Harvard):
Street, S, Cook, A, Mohammed Ali, H, Rayment, T & Davenport, A 2017, 'The effect of deposition conditions on atmospheric pitting corrosion location under Evans droplets on 304L stainless steel', *Corrosion*.
https://doi.org/10.5006/2614

Link to publication on Research at Birmingham portal

General rights
Unless a licence is specified above, all rights (including copyright and moral rights) in this document are retained by the authors and/or the copyright holders. The express permission of the copyright holder must be obtained for any use of this material other than for purposes permitted by law.

•Users may freely distribute the URL that is used to identify this publication.
•Users may download and/or print one copy of the publication from the University of Birmingham research portal for the purpose of private study or non-commercial research.
•User may use extracts from the document in line with the concept of 'fair dealing' under the Copyright, Designs and Patents Act 1988 (?)
•Users may not further distribute the material nor use it for the purposes of commercial gain.

Where a licence is displayed above, please note the terms and conditions of the licence govern your use of this document.

When citing, please reference the published version.

Take down policy
While the University of Birmingham exercises care and attention in making items available there are rare occasions when an item has been uploaded in error or has been deemed to be commercially or otherwise sensitive.

If you believe that this is the case for this document, please contact UBIRA@lists.bham.ac.uk providing details and we will remove access to the work immediately and investigate.

Download date: 05. May. 2023

The effect of deposition conditions on atmospheric pitting corrosion location under Evans droplets on 304L stainless steel

Steven R. Street[ǂ], Angus J.M.C. Cook *, Haval B. Mohammed-Ali *,**, Trevor Rayment ***, Alison J. Davenport**

**School of Metallurgy and Materials, University of Birmingham, UK*

***Department of Physics, University of Zakho, Iraq*

****School of Chemistry, University of Birmingham, UK.*

ARTICLE INFO

Article history:

Received Day Month Year (This style is Article History and Keywords)
Accepted Day Month Year
Available Day Month Year

Keywords:

A. Stainless steel
B. Atmospheric enviroments
C. differential aeration cell
D. localized corrosion
E. relative humidity
F. open-circuit potential

ǂ Corresponding author: Steven R. Street, telephone +44 121 414 5211; School of Metallurgy and Materials, University of Birmingham, Pritchatts Rd, Edgbaston, B15 2TT, UK, email: (s.r.street@bham.ac.uk).

ABSTRACT

Pit location during atmospheric corrosion of 304L stainless steel under $MgCl_2$ droplets depends on initial droplet concentration. Pits formed predominantly in the center of the droplet for concentrations ≥ 4 M, closer to the perimeter for 1.5-3 M, and were randomly distributed for concentrations ≤ 1 M. Pits initiated only after the droplets had evaporated to a critical concentration > 3 M, where droplets deposited with lower initial concentrations were thinner. The results can be explained in terms of "differential aeration" and IR drop effects, showing that corrosion in "splash zones" may differ from that under aerosol salt deposit layers that deliquesce forming initially saturated solutions.

INTRODUCTION

Atmospheric corrosion of metals occurs when small amounts of salt are deposited onto exposed surfaces. In "splash zones", dilute droplets will land on metal surfaces, and then concentrate as they equilibrate with the ambient relative humidity [1-4]. However, in other conditions, solid aerosol salt particles can accumulate on surfaces, and then deliquesce when the ambient relative humidity is sufficiently high, forming concentrated salt droplets when it initially wets [5, 6]. At equilibrium the water activity of saline solutions will equal that of the atmosphere, which is determined by the relative humidity (RH) [7]. It is therefore possible to get highly concentrated saline solutions that allow the corrosion of metals usually considered resistant to attack when immersed in dilute saline solutions. The restricted solution volume also shortens the pathway of oxygen from the air-solution interface to the metal-solution interface [8] allowing oxygen reduction reactions to continue and drive further anodic dissolution. As such, the dominant limiting factor to atmospheric corrosion propagation is generally considered to be the cathodic current [9, 10].

Dilute droplets of saline solution have long been used to simulate the effects of atmospheric corrosion. The first major discussion of corrosion under droplets was by U.R. Evans [11-13] who used NaCl with pH indicator—phenol-phthalein/potassium ferricyanide—on freshly ground mild steel to show a strong trend for anodic dissolution at the center of droplets and cathodic reactions occurring around the droplet edge. This was explained by "differential aeration", with oxygen supply to the surface of the metal being significantly easier at the edge of the droplet where it is thinner. Evans also observed that where corrosion initiated at the edge of the droplet, it slowly migrated towards the center as the passive layer there was less stable.

The Evans droplet experiment is noted to be of particular use with alloys that have less stable passive oxide layers [14, 15]. Chen and Mansfeld [16] used scanning Kelvin probe on steel to show a strong cathodic region dominates at, and beyond, the edge of a droplet. Risteen *et al*. [17] noted corrosion behavior became progressively more filiform and less Evans-like in droplets under 500 µm diameter on 1010 steel. Li and Hihara [18] observed corrosion occurring in the center of NaCl droplets on ultrapure iron for droplets with diameters greater than 200 µm. Wire beam electrode (WBE) arrays of Zn alloy [19] also indicate corrosion towards the center of droplets of sufficient size, with modelling supporting the influence of oxygen diffusion resulting in differential aeration [20].

However, the Evans droplet experiment is less useful in interpreting corrosion of alloys with stable passive oxide layers. Using large datasets, a wide range of pitting initiation sites has been observed on 316L [21] and 304L stainless steels [3], with pit location under the droplet often influencing the pit morphology. Some examples of wet/dry cycling of $MgCl_2$ droplets on 304 stainless steels have shown no strong trend in pitting location when cycled up to 6 times in both as-received [22] and sensitized [23] conditions. Long-term corrosion of 2205 duplex stainless steel has shown corrosion distributed around the droplet with significant selective dissolution of the austenite phase at the edges [24]. Aluminum alloys have generally shown pitting location to be determined by microstructure and not differential aeration [25]. Knight *et al*.[26] confirmed this when they observed that droplets of 0.6 M NaCl on AA2025 and AA7075 aluminum alloys had no preferential pitting location over a range of droplet diameters up to 10 mm, though this was not quantified. Interestingly, Oltra *et al*. [27] did see an influence of differential aeration on AA2011 aluminum alloy, observing attack around Al_2Cu intermetallic particle towards the edge of droplets of very pure water.

This was supported by the observation of increased pH in the edge regions of the droplet as compared to the center.

It has been suggested [28] that the lack of trend in position of pitting site on highly passive alloys may be due to a reduced rate of oxygen consumption on the altered passive layer, preventing differential aeration from developing in the droplet. However, WBE arrays constructed with 304 stainless steel [29] show that large droplets cause a trend in corrosion towards the droplet edge rather than the center, suggesting oxygen access does play a role. A three-phase boundary region, where oxygen is readily accessible, has been suggested to account for this [30].

Dilute droplets of saline solution have been used to simulate both splash zone and aerosol deposition scenarios despite the difference in the early stages of experimental conditions. This raises questions about the universality of the droplet deposition technique, particularly in light of recent work that has found differences when directly comparing droplets and dry salt deposition [31-35]. Highly concentrated solutions show reduced diffusivity, which hinders mass transport during pitting, and reduced ionic conductivity, which contributes to an increased IR-drop between anodic and cathodic regions [3].

Pitting initiation on stainless steel is stochastic [36-38] and conclusions from small datasets are unreliable. High-throughput methods [3, 39], where large numbers of droplets are deposited at once, allow statistical analysis to be conducted on pitting corrosion to see the influence of experimental variables. Several statistical tools exist that allow trends in categorical data to be examined and quantified [40]. The Chi-squared ($\chi 2$) test is a method of hypothesis testing commonly used in categorical datasets where sampling method is considered random. It is particularly useful in testing the "null hypothesis", i.e. that the results of a dataset are independent of a particular variable. Chi-squared tests rely on a standard distribution determined by the degrees of freedom in the dataset, and produce a probability that the null hypothesis is true. The binomial standard deviation is also used on categorical data where just two outcomes are possible and where the results are independent from each other. This technique gives a range of the variability of a dataset from the mean.

This study investigates the influence of deposition conditions on pitting location under droplets of $MgCl_2$ on 304L stainless steel. High-throughput methods are used to collect large volumes of data so that statistical techniques can be applied to determine trends in pitting location.

EXPERIMENTAL

Droplet Array Experiments

Cold-rolled and solution-annealed 304L stainless steel (Table 1) was supplied as 3 mm thick plates (Aperam, France). The plate was cut into samples of either 75 mm x 25 mm or 25 mm x 25 mm and ground using P800 grit paper with the final pass in the direction perpendicular to the rolling direction of the plate. The samples were then ultrasonically cleaned in deionized (DI) water for 15 minutes, rinsed in DI water and blown dry using a hand-squeezed air bottle. Samples were then left for 24 hours in covered ambient conditions before deposition of droplets to allow the formation of a passive film.

Arrays of 2 µl droplets of $MgCl_2$, made from $MgCl_2.6H_2O$ (Sigma-Aldrich), were deposited on samples using a Multiprobe II liquid handling system (Perkin-Elmer Life Sciences) at 5 mm intervals. 20 – 60 droplets of a single concentration were deposited on each sample, arrays taking less than 8 minutes to deposit in all cases. Droplets were deposited with needle tip 0.91 mm from metal surface at 10 µls-1. Laboratory conditions were between 20–23 °C and 25–44% RH.
The influence of relative humidity (RH) was investigated by depositing droplets of 0.27 M $MgCl_2$ and holding each plate in 33%, 38%, 43%, 48%, 53%, or 59% RH for 24 hours in an atmospheric chamber (ECO135, TAS Ltd). The influence of initial droplet concentration was investigated by depositing droplets of 0.14 M, 0.27 M, 1 M, 1.5 M, 2.3 M, 4 M, 4.5 M or 5 M $MgCl_2$ droplets and holding them at 33% RH for 24 hours in an atmospheric chamber. Temperature was fixed at 30 ± 1 °C for all samples. The number of droplets deposited for each condition ranged from 40-100 and is indicated in the results section.

Ag Wire Reference Electrode Experiments

Electrochemistry experiments were conducted using Ag wire electrodes following the method of Nam *et al*. [22]. Ag wire of 50 µm diameter was rinsed in DI water and suspended above a 304L stainless steel plate that was prepared as described above (Figure 1a). The wire was clamped and held under tension on top of PTFE tape approximately 40 µm above the sample surface (Figure 1b). 4 wires were held across the sample to test different $MgCl_2$ concentrations.

The sample was then placed in an atmospheric chamber (ECO135, TAS Ltd) and held at 30 ± 1 °C and 33 ± 2 %RH. The Ag wire was connected to a two-electrode CompactStat potentiostat (Ivium), with the sample acting as the working electrode with a time resolution of 1 s. A droplet of 1 M $MgCl_2$ was deposited on the sample, touching one wire. This was repeated with 2 M, 3 M, and 4 M $MgCl_2$ on separate wires.

Unanodized Ag wire was used for these experiments as reference electrode instead of a standard reference electrode or Luggin probe. This was to allow the distance between the stainless steel surface and the reference to be well-controlled, which is necessary when dealing with such thin layers of solution. As discussed by Nam *et al*.[22], Ag wire is not suitable for measuring accurate corrosion potentials under these conditions as the potential of the silver electrode, E_{Ag}, changes with solution concentration as the droplet reaches equilibrium with the atmosphere. However, the technique is suitable for ranking corrosion potentials and recording dramatic changes in potential, e.g. when pitting initiates.

Ag wires used as quasi-reference electrodes could be anodized first to maintain a AgCl film on the surface. However, the film generated by anodizing dissolves after a short time in concentrated $MgCl_2$ solutions. Futhermore, the amount of AgCl needed to coat the Ag wire and maintain a reversible reference electrode may result in large amounts of Ag-Cl complex ions inside the droplet, which risks affecting pitting behaviour. Unanodized Ag is therefore the best option for these conditions. It is recognized, however, that the potential measured here are not potentials because E_{Ag} does change with solution concentration during experiment.

Statistical Analysis of Droplet Arrays

Droplets take up an approximately elliptical shape at and after deposition (Figure 2a), elongated along the grinding lines of the plate. The major, 2a, and minor, 2b, axes of each droplet were measured using the initial droplet area, allowing the construction of an elliptical perimeter. The distance and angle of the pit center from the center of the ellipse was measured. Pit center was determined to be the center of the shallow dish region [3, 41, 42], which is the morphological feature that appears during initiation of pitting under atmospheric conditions on stainless steels.
The ellipse was then divided into two regions of equal area: an internal ellipse that has semi-major axis of a/√2 and semi-minor axis of b/√2 (inner region), and an outer annulus of equal area (outer region) (Figure 2b). Using the measured distance, L, and angle, θ, of the pit from the center of the droplet, the location of the pit was determined algebraically to see if it was in the inner or outer region, i.e. if the pit is in the inner region,

$$\frac{(Lcos\theta)^2}{\left(\frac{a}{\sqrt{2}}\right)^2} + \frac{(Lsin\theta)^2}{\left(\frac{b}{\sqrt{2}}\right)^2} \leq 1 \qquad (1)$$

Otherwise, the pit is considered to be in the outer region. This accommodates where the actual droplet perimeter extends outside the calculated droplet perimeter.

Analysis of pitting location in this way generates "categorical" data, i.e. each datum will fall into one of two categories. This allows for statistical techniques that employ categorical data to be used to interpret the pitting location. A "null hypothesis" approach was used where it was assumed that there is no relationship between a pit's initiation site and its location under the droplet. By defining the equally sized regions to be at the edge (outer) and at the center (inner) of the droplet, the influence of droplet thickness and "differential aeration" caused by oxygen diffusion limitation can be investigated. A bias of results in favor of either region would indicate a relationship between pitting and location. Two statistical methods are used to analyze the validity of the null hypothesis:

- Chi-squared (χ^2) test gives the probability, H_0, of these data agreeing with the null hypothesis (assuming a degree of freedom of 1). H_0 values of greater than 5% are generally considered to show no significant statistical variation from the null hypothesis, meaning no trend in pitting position
- Binomial standard deviation, σ_{H0}, which gives the expected standard deviation for the data set given that the null hypothesis is correct (i.e. p=0.5).

RESULTS

Effect of changes in Relative Humidity (RH)

The results of different exposure humidities on droplets that were 2 µl volume and 0.27 M $MgCl_2$ at deposition are summarized in Table 2. Figure 3 shows the results of pitting for droplets exposed to humidities between 33% RH and 59% RH. Between 33% RH and 53% RH, the variation between the null hypothesis and the recorded results falls within σ_{H0}, or one binomial standard deviation. At 59% RH, results lies within $2\sigma_{H0}$ showing a slight trend for edge initiation. Figure 4 shows a strong probability for satisfying the null hypothesis when relative humidity is held at or below 53% RH. At 59% RH, the probability of satisfying H_0 is only 14%, but this is still above the 5% threshold usually considered for determining statistical relevance in χ^2 tests, so can still be considered to have a low probability of a trend in data.

Effect of solution concentration at deposition

The results of different initial solution concentrations of $MgCl_2$ of 2 µl droplets are summarized in Table 3. Results in Figure 5 show that at low initial concentrations, between 0.14 M and 1 M $MgCl_2$, all data fall well within σ_{H_0} of 50% of droplets pitting in the inner region. The probability of satisfying the null hypothesis (H_0) at these concentrations is high (Figure 6), which supports this observation. When deposition concentration increases and is between 1.5 M and 3 M $MgCl_2$ a distinct trend develops for more pits to be initiated in the outer region of the droplet, i.e. towards the edge. In highly concentrated solutions between 4 M and 5 M $MgCl_2$ this trend reverses, and pitting occurs most often in the inner region, i.e. towards the center of the pit. The H_0 probability (Figure 6) for concentrations 1.5 M to 5 M $MgCl_2$ is less than 1 % in all cases, making the null hypothesis unlikely.

Ag wire electrochemistry

Ag wires have been used to study the initiation times after deposition of droplets with different deposition concentrations. An example is shown in Figure 7 where a Ag wire can be seen on the right-hand side of the droplet. Results for 2 µl droplets of 1 M to 4 M $MgCl_2$ solutions were tested in each case (Figure 8). When 4 M $MgCl_2$ was deposited, pitting began virtually immediately with only a momentary rise in potential before initiation. 2 M and 3 M $MgCl_2$ droplets showed momentary drops in potential before pitting finally initiated, with 3 M droplet pitting after 50 s and 2 M droplet after 180 s. 1 M $MgCl_2$ droplet pitted after 320 s. The fluctuations in potential observed 2 M and 3 M before pitting did not occur in 1 M, and potential was seen to reduce for a period after deposition (between 50 s and 120 s) then increase again until pitting initiated.

Droplet heights at deposition and at equilibrium

Typical heights for droplets at deposition and at equilibrium with 60% RH and 33% RH are shown in Table 4, with 60% RH being the approximate RH where initiation occurs on this alloy, and 33% Rh being the deliquescence humidity of $MgCl_2$. Droplets with initial concentrations of 4 M $MgCl_2$ and greater were not measured at 60% RH as this would have diluted the droplets. Heights of less than 100 µm are unable to be measured with accuracy.

While initial droplet heights are broadly similar for all concentrations, droplets with low initial solution concentrations reduce in height significantly by the time they reach equilibrium with 60%RH, which is the approximate humidity that initiation occurs. Droplets with initial concentrations of 4 M and higher are observed to have significant spreading after deposition.

DISCUSSION

Three distinct trends are observed in pitting, relating to the deposition concentration of the droplet (Figure 9).

1. At low deposition concentrations, pits initiate at random locations under a droplet.
2. At higher concentrations but where initiation is not immediate, pitting is more likely to occur near the droplet edge.
3. At concentrations that allow initiation to begin immediately, pitting is more likely to occur near the center of the droplet.

The thickness of the droplet at the moment of initiation is an important factor when seeking to understand these three trends in behavior observed as deposition concentration increases. To support pitting in the crucial early moments of attack, a sufficiently high potential and current are required to sustain an active chemistry. Under droplets this translates to having both a sufficiently large cathode area, as these systems are generally considered to be cathodically limited [9, 10], and a sufficiently conductive pathway (reduced IR-drop) between the anode and cathode.

Trend 1: Random pitting location

Droplets deposited with a dilute initial solution concentrations must lose significant amounts of water to be at equilibrium with low relative humidities, creating very thin droplet layers. When the droplets are at solution concentrations high enough to allow pitting to initiate, which is suggested to occur at between 58% RH (3.5 M) to 47% RH (4.1 M $MgCl_2$) if at equilibrium [3] [22], the droplet will be very thin. These thin droplets allow easy oxygen access all over the metal surface, permitting strongly cathodic regions to occur anywhere. However, thin droplets also cause a large IR-drop, meaning pitting must be near strongly cathodic regions. Thus, pitting can initiate anywhere on the droplet surface at sites determined metallurgically, not by differential aeration.

Droplets with deposition concentrations of 0.14 M – 1 M in 33% RH show no preferential region in pitting location. Those with deposition concentration of 0.27 M in RH between 33%-53% also show no preference. All sets are within $2\sigma_{H0}$ of the null hypothesis—that there is no preference in pitting location (Figure 3 and Figure 5)—and

H_0 probability is high (i.e. above 5%) in all cases (Figure 4 and Figure 6), indicating that the null hypothesis is reasonable.

Trend 2: Edge pitting

Droplets with deposition concentrations of 1.5 M – 3 M $MgCl_2$ show a strong trend towards pitting at the edge of the droplet. The data were more than 2σ from the assumed distribution. H_0 probability is less than 1% in each case, indicating very weak likelihood that the null hypothesis is true. Competition between pitting sites exists, as seen by metastable pitting on Ag wire (Figure 8). The concentrations of these droplets are not aggressive enough to initiate immediately upon deposition.

When initiation does begin, it is likely that the droplets are still thick enough to reduce availability of oxygen to center of droplet compared to the edge, making stronger cathodes appear towards the edge. The droplets may still have a large IR-drop, so pitting must initiate near a strong cathode, i.e. at the edge.

Droplets with 0.27 M deposition concentration in 59% RH also show a slight trend towards edge initiation. Data fall between σ and 2σ of the null hypothesis, and H_0 probability is reduced to 14%. Although this is higher than the prescribed 5% "significance threshold", is not as high as other data of the same deposition concentration. This may be because the initiation time is longer at this RH as this is on the cusp of the initiation regime, and as such has a slightly thicker droplet at initiation, causing differential aeration in some cases [3].

Trend 3: Center pitting

Droplets of deposition concentration 4 M – 5 M $MgCl_2$ show a strong trend for pitting towards the center (Figure 5), a similar pattern to the Evans droplet model [11]. Pitting begins quickly in these concentrations, as shown by Ag wire experiments (Figure 8). As these solutions are deposited at a concentration above that required for initiation to occur, all possible initiation sites will compete at deposition. This attack, combined with the increase in passive current densities at high concentrations [3], will deplete dissolved oxygen within the droplet rapidly, resulting in an oxygen concentration gradient inside the droplet. Electrochemistry on stainless steels [3] has shown that in concentrations above 3.5 M $MgCl_2$, which is broadly where pitting starts on 304L, there is no metastable pitting and no sharp and clearly defined pitting potential. Instead, there is a gradual increase in current during pitting. This may be due to initiation of a large number of metastable pits. Even though only a single pit may be present, attack at numerous inclusions can occur, rapidly consuming dissolved oxygen. In this way, initiation causes differential aeration.

Oxygen solubility and diffusivity are also slower at these concentrations [3, 43], so replenishing the oxygen in solution near the surface is difficult once it is consumed. No competition between initiation sites is seen in the Ag wire experiments, possibly due to the low temporal resolution (1 s) which limits the ability to observe these events as they can be seen more clearly on shorter timescales [44]. Although conductivity is reduced at high concentration, conductance is increased due to the thick droplet layer, allowing anodes easier ionic pathways to the cathodic areas. This would allow large cathodic currents to be accessed towards the center of the droplet.

Evans Droplet Model

Evans stated that, under NaCl droplets, "in the case of iron and steel, the distribution of anodic and cathodic areas is determined almost entirely by the oxygen-distribution in the liquid, and only to a small extent on the composition or physical character of the different portions of the metal"[11]. He later refined these observations [12], describing small localized anodic and cathodic areas initially dispersed all over the metal surface under the droplet, but once the dissolved oxygen was consumed and an oxygen concentration gradient had developed in the droplet, the anodic sites converged at the center and the edge of the droplet acted as the cathode. This mechanism also provided an explanation of the death of anode sites near the edge, with any iron ions released near the edge being deposited as solid hydroxides or oxides at the surface and "healing" the anodic sites. Stainless steels, however, have very stable passive layers and the corrosion location cannot migrate around the metal surface during growth. Initiation has been strongly linked with metallurgy and local inclusion chemistry, particularly with sulphides [45, 46], and propagation with occluding morphologies to maintain a critical chemistry [47]. This, in concert with drop in potential when pitting starts and the cathodic protection of the rest of the pit surface, makes the drifting of pit location difficult. As observing more than one pitting site is rare after 24 hours, it can be assumed that the stability of pits under the conditions tested is sufficient to overcome other factors that would driving pitting to occur towards the center of the droplet. As such, factors that generate a trend in location must occur early during the initiation stages of pitting, not during continual corrosion such as Evans witnessed on Fe.

Aerosol vs Splash Zone deposition

These results show a difference in pitting behavior depending on whether droplets are deposited as concentrated or as dilute solutions. This is in essence simulating the difference between aerosol deliquescence conditions, where deposited particulate salts draw in moisture to form concentrated solutions [34], and splash zone conditions, where salt water splashes onto surfaces and dries as its water activity reaches equilibrium with the atmosphere.
Aerosol conditions, where droplets start at or near saturation, have very small initiation times and show evidence of rapid consumption of saturated oxygen. Pit initiation is determined not only by metallurgy but by oxygen gradients inside the solution. Splash zone conditions, where dilute solutions are deposited, have their pitting location determined entirely through metallurgy. Evidence for variation in corrosion behavior has been observed when comparing droplets and salt particles of NaCl, $MgCl_2$, and ASTM standard sea water [31, 32, 48]. Recent literature has shown instances where dilute droplets have been used to investigate corrosion regimes known to be caused by aerosol contamination, e.g. nuclear waste storage [1-4]. The current work further emphasizes the need to appreciate the difference in aerosol and splash zone deposition in atmospheric corrosion particularly in early stages.

CONCLUSIONS

For atmospheric corrosion under droplets of $MgCl_2$ on 304L stainless steel, deposition conditions influence pitting location.

- Pitting tends to take place towards the center of the droplet when the initially-deposited $MgCl_2$ concentration is ≥4 M. This may be attributed to rapid consumption of dissolved oxygen and low values for its solubility and diffusivity in concentrated droplets, leading to the cathodic reaction taking place predominantly at the edge of the droplet. This can be regarded as a case of "differential aeration" similar to the observations of Evans for corrosion of carbon steel.

- When $MgCl_2$ droplets are deposited with an initial concentration between 1.5 and 3 M, pitting occurs towards the edge of the droplet. Under these conditions, it the droplet must evaporate before the critical concentration for pit initiation is reached, and is thus thinner than the 4 M droplet. At the same time, oxygen depletion is still expected, and so the cathodic reaction is likely to take place predominantly at the edge of the droplet. However, in

this case, the droplet is thinner, so there is significant IR drop, so pitting is favored closer to the cathode.

- For initial droplet concentrations of 0.14 and 1 M, pitting occurs in random locations. In these cases, the droplet evaporates for longer times and becomes very thin before the critical concentration of for pitting is reached. Oxygen is able to diffuse more readily across such thin layers, so "differential aeration" does not occur.

- These observations suggest that development of atmospheric corrosion may be different for "splash zone" conditions where there is direct deposition of droplets (e.g. where there is sea spray), compared with conditions where salt aerosol particles accumulate on metal surfaces and subsequently deliquesce to form droplets.

REFERENCES

1. M. Gunther, N.P.C. Stevens, G. McFiggans, A.B. Cook, Corrosion Engineering Science and Technology 49, 6 (2014): p. 509-513.
2. O.E. Albores-Silva, E.A. Charles, C. Padovani, Corrosion Engineering Science and Technology 46, 2 (2011): p. 124-128.
3. S.R. Street, N. Mi, A.J.M.C. Cook, H.B. Mohammed-Ali, L. Guo, T. Rayment, A.J. Davenport, Faraday Discussions, (2015):
4. C. Padovani, O.E. Albores-Silva, E.A. Charles, Corrosion 71, 3 (2015): p. 292-304.
5. G.G. Scatigno, M.P. Ryan, F. Giuliani, M.R. Wenman, Materials Science and Engineering a-Structural Materials Properties Microstructure and Processing 668, (2016): p. 20-29.
6. D.T. Spencer, M.R. Edwards, M.R. Wenman, C. Tsitsios, G.G. Scatigno, P.R. Chard-Tuckey, Corrosion Science 88, (2014): p. 76-88.
7. T. Choosri, G. Koglbauer, M. Wendland, J. Chem. Eng. Data 54, 4 (2009): p. 1179-1182.
8. N.D. Tomashov, Corrosion 20, 1 (1964): p. 7t-14t.
9. Z.Y. Chen, F. Cui, R.G. Kelly, Journal of the Electrochemical Society 155, 7 (2008): p. C360-C368.
10. Z.Y. Chen, R.G. Kelly, Journal of the Electrochemical Society 157, 2 (2010): p. C69-C78.
11. U.R. Evans, Metal Industry 29, (1926): p. 481-482.
12. U.R. Evans, The Corrosion and Oxidation of Metals, 1st ed.(London: Edward Arnold Ltd., 1960).
13. U.R. Evans, Industrial & Engineering Chemistry 17, 4 (1925): p. 363-372.
14. S.X. Li, L.H. Hihara, Journal of the Electrochemical Society 159, 11 (2012): p. C461-C468.
15. A.K. Neufeld, I.S. Cole, A.M. Bond, S.A. Furman, Corrosion Science 44, 3 (2002): p. 555-572.
16. C.Y. Chen, F. Mansfeld, Corrosion Science 39, 2 (1997): p. 409-413.
17. B.E. Risteen, E. Schindelholz, R.G. Kelly, Journal of the Electrochemical Society 161, 14 (2014): p. C580-C586.
18. S.X. Li, L.H. Hihara, Corrosion Science 108, (2016): p. 200-204.
19. T.H. Muster, A. Bradbury, A. Trinchi, I.S. Cole, T. Markley, D. Lau, S. Dligatch, A. Bendavid, P. Martin, Electrochimica Acta 56, 4 (2011): p. 1866-1873.
20. I.S. Cole, N.S. Azmat, A. Kanta, M. Venkatraman, Int. Mater. Rev. 54, 3 (2009): p. 117-133.
21. A.J.M.C. Cook, C. Padovani, A.J. Davenport, Journal of the Electrochemical Society 164, 4 (2017): p. C148-C163
22. T.V. Nam, E. Tada, A. Nishikata, Journal of the Electrochemical Society 162, 9 (2015): p. C419-C425.
23. C.Q. Cheng, L.I. Klinkenberg, Y. Ise, J. Zhao, E. Tada, A. Nishikata, Corrosion Science 118, (2017): p. 217-226.
24. C. Ornek, X.L. Zhong, D.L. Engelberg, Corrosion 72, 3 (2016): p. 384-399.
25. P.C. King, I.S. Cole, P.A. Corrigan, A.E. Hughes, T.H. Muster, Corrosion Science 53, 3 (2011): p. 1086-1096.
26. S.P. Knight, A.D. Sudholz, A. Butler, S. Palanisamy, M.S. Dargusch, A.R. Trueman, Materials and Corrosion-Werkstoffe Und Korrosion 67, 12 (2016): p. 1294-1307.
27. R. Oltra, B. Malki, F. Rechou, Electrochimica Acta 55, 15 (2010): p. 4536-4542.
28. G. Frankel, G. Thornton, S. Street, T. Rayment, D. Williams, A. Cook, A. Davenport, S. Gibbon, D. Engelberg, C. Ornek, A. Mol, P. Marcus, D. Shoesmith, C. Wren, K. Yliniemi, G. Williams, S. Lyon, R. Lindsay, T. Hughes, J. Lutzenkirchen, S.-T. Cheng, J. Scully, S.F. Lee, R. Newman, C. Taylor, R. Springell, J. Mauzeroll, S. Virtanen, S. Heurtault, J. Sullivan, Faraday Discussions 180, 0 (2015): p. 381-414.
29. Y.H. Wang, W. Wang, Y.Y. Liu, L. Zhong, J. Wang, Corrosion Science 53, 9 (2011): p. 2963-2968.
30. J. Jiang, J. Wang, Y.H. Lu, J.Z. Hu, Electrochimica Acta 54, 5 (2009): p. 1426-1435.
31. E. Schindelholz, B.E. Risteen, R.G. Kelly, Journal of the Electrochemical Society 161, 10 (2014): p. C450-C459.
32. E. Schindelholz, B.E. Risteen, R.G. Kelly, Journal of the Electrochemical Society 161, 10 (2014): p. C460-C470.
33. N. Mi, M. Ghahari, T. Rayment, A.J. Davenport, Corrosion Science 53, 10 (2011): p. 3114-3121.
34. S.X. Li, L.H. Hihara, Corrosion Engineering Science and Technology 45, 1 (2010): p. 49-56.
35. A. Ul-Hamid, H. Saricimen, A. Quddus, A.I. Mohammed, L.M. Al-Hems, Corrosion Engineering Science and Technology 52, 2 (2017): p. 134-140.
36. T. Shibata, T. Takeyama, Corrosion 33, 7 (1977): p. 243-251.
37. D.E. Williams, C. Westcott, M. Fleischmann, Journal of the Electrochemical Society 132, 8 (1985): p. 1796-1804.
38. D.E. Williams, C. Westcott, M. Fleischmann, Journal of the Electrochemical Society 132, 8 (1985): p. 1804-1811.
39. N.S. Azmat, K.D. Ralston, T.H. Muster, B.C. Muddle, I.S. Cole, Electrochemical and Solid State Letters 14, 6 (2011): p. C9-C11.
40. E. Kreyszig, Advanced Engineering Mathematics, 9th ed.(Hoboken, NJ: John Wiley, 2006).
41. S. Hastuty, A. Nishikata, T. Tsuru, Corrosion Science 52, 6 (2010): p. 2035-2043.
42. B. Maier, G.S. Frankel, Journal of the Electrochemical Society 157, 10 (2010): p. C302-C312.
43. OLI Systems, in Oli Analyzer 9.0, ed., vol. 9.0 2013).
44. R.S. Lillard, G. Vasquez, D.F. Bahr, Corrosion 66, 7 (2010):
45. E.G. Webb, R.C. Alkire, Journal of the Electrochemical Society 149, 6 (2002): p. B272-B279.
46. J. Stewart, D.E. Williams, Corrosion Science 33, 3 (1992): p. 457-474.
47. J.R. Galvele, Journal of the Electrochemical Society 123, 4 (1976): p. 464-474.
48. J. Zhang, J. Wang, Y. Wang, Corrosion 61, 12 (2005): p. 1167-1172.

ACKNOWLEDGEMENTS

Steven Street is funded by the School of Metallurgy and Materials (University of Birmingham) and Diamond Light Source, Ltd.

FIGURE CAPTIONS

FIGURE 1 Ag wire cell used to detect corrosion initiation under droplets of $MgCl_2$. (a) 2 µl Droplets of $MgCl_2$ with concentrations indicated were deposited on 304L stainless steel at 30 °C in 33% RH inside an atmospheric chamber. Droplets were deposited and measured using a CompactStat potentiostat. (b) Side view of Ag wire suspended approx. 40 µm above sample by being clamped under tension on PTFE tape.

Figure 2 (a) Measurement of angle, θ, and distance of pit, L, from ellipse center. Ellipse outline was calculated using general equation of an ellipse. 2 µl droplet of 0.27 M $MgCl_2$ solution was held at 30 °C and 33% RH on 304L stainless steel for 24 hours, (b) calculation of A_{inner} and A_{outer} regions using measured semi-major axis, a, and semi-minor axis, b, for each droplet.

FIGURE 3 Percentage of pits that occurred in each region under 2 µl droplets of 0.27 M $MgCl_2$ on 304L stainless steel at 30 °C in different RH. Error bars are binomial standard deviation, σ_{H_0}, expected of each set assuming the null hypothesis. Null hypothesis probability, H_0, marked with dotted line.

FIGURE 4 Probability that the null hypothesis (H_0) is satisfied, i.e. that pitting is unrelated to position under a droplet, of datasets of 2 µl droplets of 0.27 M $MgCl_2$ on 304L stainless steel at 30 °C in different RH. Degrees of freedom, df=1.

FIGURE 5 Percentage of pits that occurred in each region under 2 µl droplets of $MgCl_2$ at 33% RH on 304L stainless steel at 30 °C at different deposition concentrations. Error bars are binomial standard deviation, σ_{H_0}, expected of each set assuming the null hypothesis. Null hypothesis probability, H_0, marked with dotted line.

FIGURE 6 Probability that the null hypothesis (H_0) is satisfied of datasets of 2 µl droplets of varying $MgCl_2$ concentration on 304L stainless steel at 30 °C in 30% RH. Degrees if freedom, df=1

FIGURE 7 2 µl droplet of $MgCl_2$ solution immediately after deposition on 304L stainless steel. Ag wire can be seen on the right-hand side of the droplet.

FIGURE 8 Potential difference data of Ag wire electrodes of 2 µl droplets of $MgCl_2$. Droplets deposited at 30 °C in 33% RH atmospheric chamber. Droplet concentrations at deposition are labelled. Time of deposition is 0 s in each case.

FIGURE 9 Pitting location trends as a function of solution concentration of droplet at deposition and equivalent equilibrium relative humidity. Data on concentrations where initiation occurs from [22]. Relative humidity data from [3].

TABLE CAPTIONS

TABLE 1 Foundry specifications of composition if 304L plate used in atmospheric corrosion experiments

TABLE 2 Quantitative results of pitting location of 2 µl droplets of 0.27 M $MgCl_2$ held at 30 °C on 304L stainless steel at 30 °C in different RH. Exposure time is 24 hours in each case. Degrees of freedom (df) of H_0 is 1.

TABLE 3 Quantitative results of pitting location of 2 µl droplets with varying concentration $MgCl_2$ held at 30 °C on 304L stainless steel at 30 °C in 33% RH. Exposure time of 24 hours in each case. Degrees of freedom (df) of H_0 is 1.

Figures

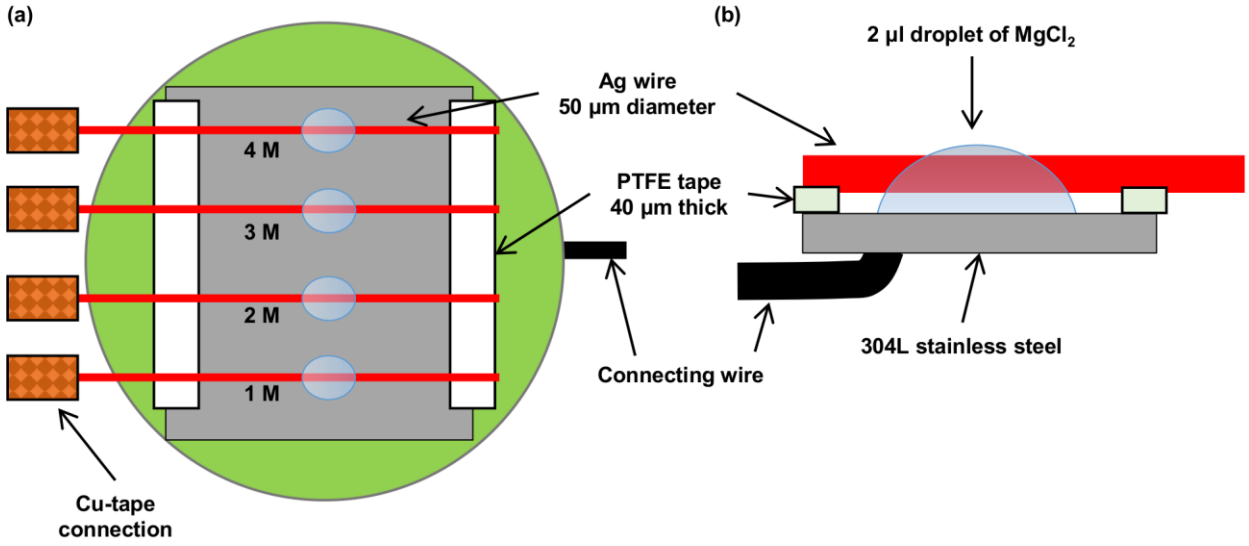

Figure 1 Ag wire cell used to detect corrosion initiation under droplets of $MgCl_2$. (a) 2 µl Droplets of $MgCl_2$ with concentrations indicated were deposited on 304L stainless steel at 30 °C in 33% RH inside an atmospheric chamber. Droplets were deposited and measured using a CompactStat potentiostat. (b) Side view of Ag wire suspended approx. 40 µm above sample by being clamped under tension on PTFE tape.

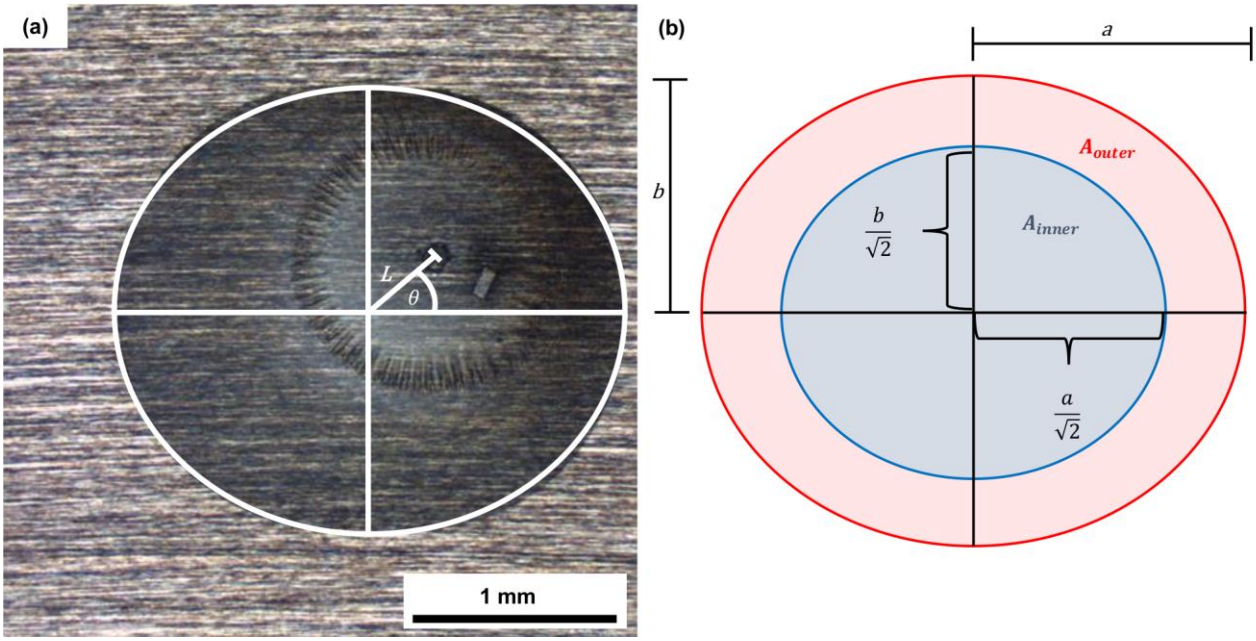

Figure 2 (a) Measurement of angle, ϑ, and distance of pit, *L*, from ellipse center. Ellipse outline was calculated using general equation of an ellipse. 2 µl droplet of 0.27 M $MgCl_2$ solution was held at 30 °C and 33% RH on 304L stainless steel for 24 hours, (b) calculation of A_{inner} and A_{outer} regions using measured semi-major axis, *a*, and semi-minor axis, *b*, for each droplet.

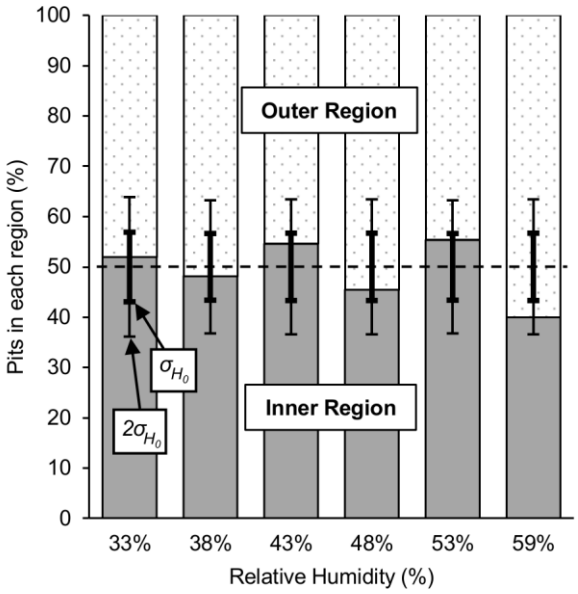

Figure 3 Percentage of pits that occurred in each region under 2 µl droplets of 0.27 M $MgCl_2$ on 304L stainless steel at 30 °C in different RH. Error bars are binomial standard deviation, σ_{H_0}, expected of each set assuming the null hypothesis. Null hypothesis probability, H_0, marked with dotted line.

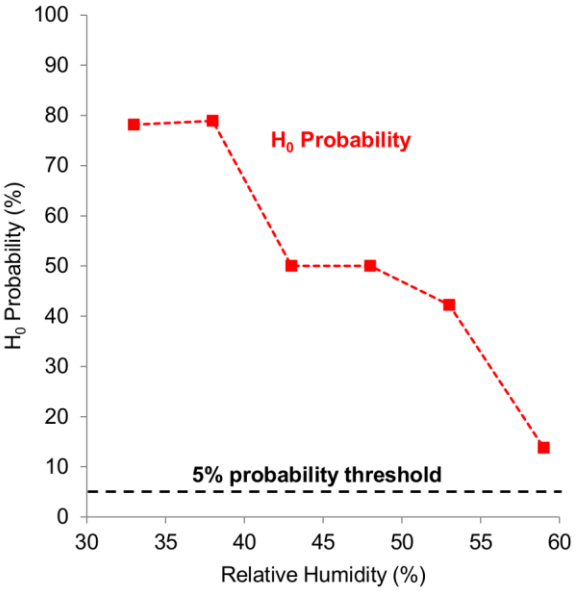

Figure 4 Probability that the null hypothesis (H_0) is satisfied, i.e. that pitting is unrelated to position under a droplet, of datasets of 2 µl droplets of 0.27 M $MgCl_2$ on 304L stainless steel at 30 °C in different RH. Degrees of freedom, df=1.

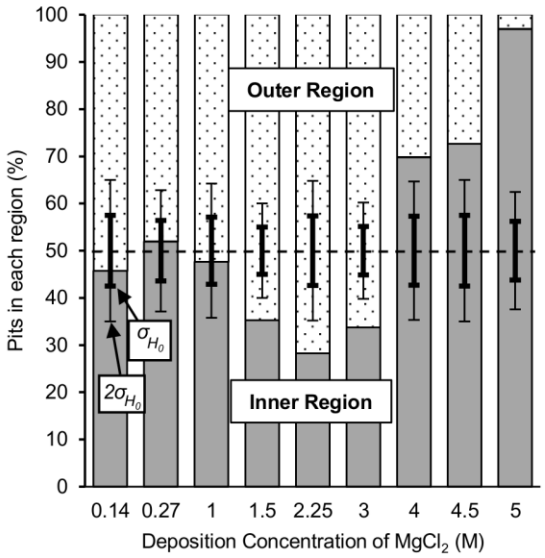

Figure 5 Percentage of pits that occurred in each region under 2 µl droplets of $MgCl_2$ at 33% RH on 304L stainless steel at 30 °C at different deposition concentrations. Error bars are binomial standard deviation, σ_{H_0}, expected of each set assuming the null hypothesis. Null hypothesis probability, H_0, marked with dotted line.

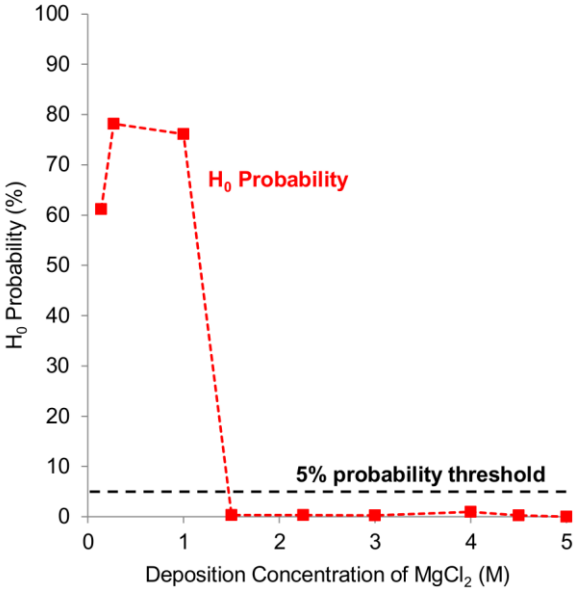

Figure 6 Probability that the null hypothesis (H_0) is satisfied of datasets of 2 µl droplets of varying $MgCl_2$ concentration on 304L stainless steel at 30 °C in 30% RH. Degrees if freedom, df=1

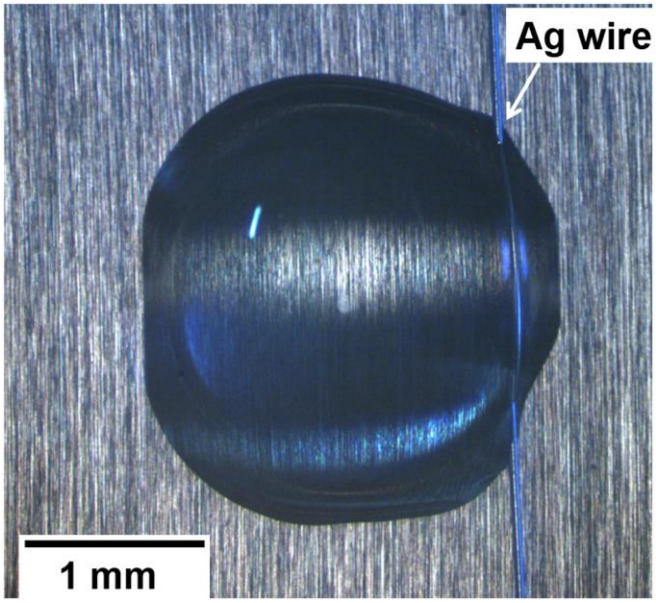

Figure 7 2 µl droplet of $MgCl_2$ solution immediately after deposition on 304L stainless steel. Ag wire can be seen on the right-hand side of the droplet.

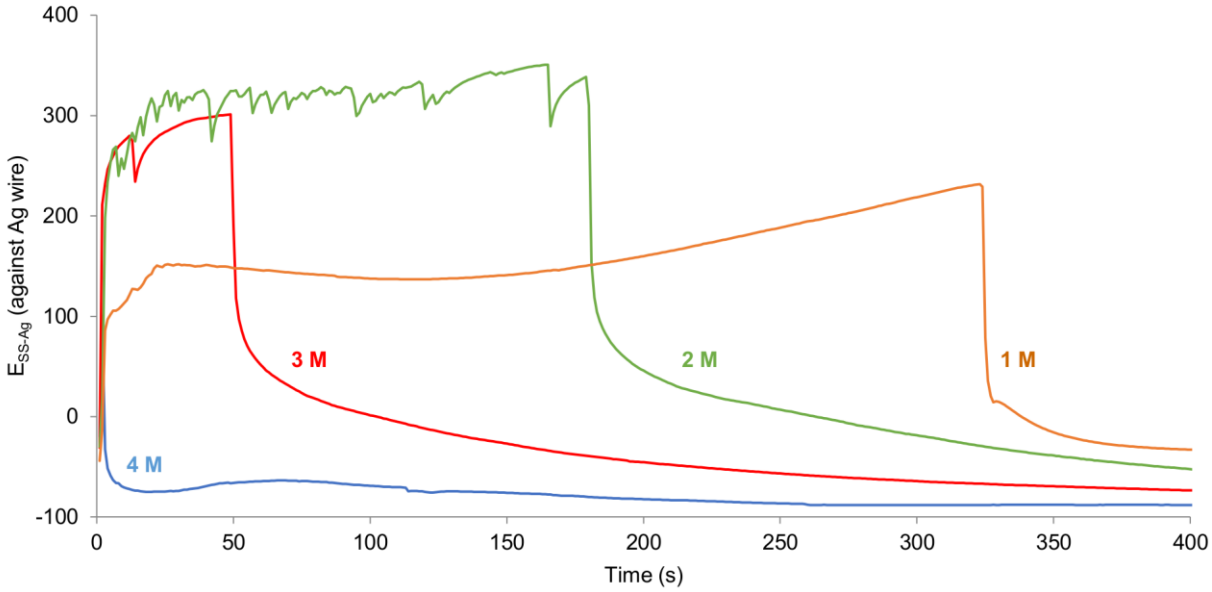

Figure 8 Potential difference data of Ag wire electrodes of 2 µl droplets of $MgCl_2$. Droplets deposited at 30 °C in 33% RH atmospheric chamber. Droplet concentrations at deposition are labelled. Time of deposition is 0 s in each case.

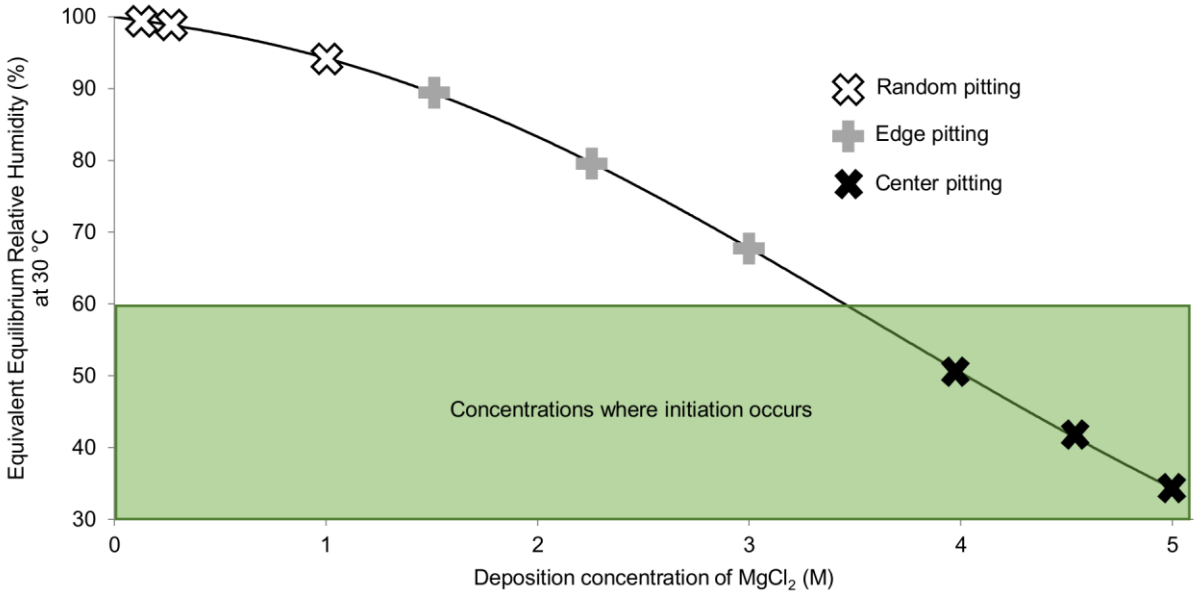

Figure 9 Pitting location trends as a function of solution concentration of droplet at deposition and equivalent equilibrium relative humidity. Data on concentrations where initiation occurs from [22]. Relative humidity data from [3].

Tables

Table 1 Foundry specifications of composition if 304L plate used in atmospheric corrosion experiments

Element (wt %)	Fe	Ni	Cr	Mn	S	C	Si	N	P
Foundry spec. (max)	Bal.	8-10.5	18-19.5	2	0.015	0.03	0.75	0.1	0.045
Foundry analysis	Bal.	8	18.08	1.46	0.0033	0.023	0.44	0.072	0.032

Table 2 Quantitative results of pitting location of 2 µl droplets of 0.27 M $MgCl_2$ held at 30 °C on 304L stainless steel at 30 °C in different RH. Exposure time is 24 hours in each case. Degrees of freedom (df) of H_0 is 1.

RH	33%	38%	43%	48%	53%	59%
Number of droplets	56	56	60	56	56	56
Total pitted (n)	52	56	55	55	56	55
Outer region	25	29	25	30	25	33
Inner region	27	27	30	25	31	22
Chi squared (χ^2)	0.077	0.071	0.45	0.45	0.64	2.2
H_0 Probability (%), df=1	78	79	50	50	42	14
H_0 Standard Deviation (σ_{H0})	3.6	3.7	3.7	3.7	3.7	3.7

Table 3 Quantitative results of pitting location of 2 µl droplets with varying concentration $MgCl_2$ held at 30 °C on 304L stainless steel at 30 °C in 33% RH. Exposure time of 24 hours in each case. Degrees of freedom (df) of H_0 is 1.

Deposition Concentration (M)	0.14	0.27	1	1.5	2.25	3	4	4.5	5
Number of droplets	40	56	45	100	46	86	45	44	66
Total pitted (n)	35	52	42	99	46	86	43	44	66
Outer region	19	25	22	64	33	57	13	12	2
Inner region	16	27	20	35	13	29	30	32	64
Chi squared (χ^2)	0.26	0.08	0.1	8.5	8.7	9.1	6.7	9.1	58
H_0 Probability (%), df=1	61	78	76	0.35	0.31	0.25	0.94	0.25	0
Standard Deviation (σ_{H0})	3	3.6	3.2	5	3.4	4.4	3.3	3.3	4.1

Table 4 Height of 2 µl droplets of $MgCl_2$ of different deposition concentration when deposited, held at equilibrium at 60% RH and at 33% RH. Droplets with initial concentrations of 4, 4.5, and 5 M $MgCl_2$ were not held at 60% RH as this would dilute the droplets. Droplets under 100 µm are unable to be measured accurately due to camera limitations. Droplets marked with * showed significant lateral spreading after deposition.

Deposition $MgCl_2$ Concentration of Droplet (M)	Droplet height at deposition (µm)	Droplet height at 60% RH (µm)	Droplet height at 33% RH (µm)
5	1060	-	690*
4.5	1000	-	610*
4	970	-	570*
3	1000	740	530
2.25	920	620	400
1.5	950	400	370
1	890	290	250
0.27	890	110	<100
0.14	910	<100	<100